Optically Detected Magnetic Resonance in Amorphous Semiconductors

JAPANESE JOURNAL OF APPLIED PHYSICS
VOL. 22, NO. 3, MARCH, 1983 pp. 375–388

—Invited Paper—

Optically Detected Magnetic Resonance in Amorphous Semiconductors

Kazuo MORIGAKI

Institute for Solid State Physics, University of Tokyo, Roppongi, Tokyo 106

(Received August 20, 1982; accepted for publication December 18, 1982)

The principle of optically detected magnetic resonance (ODMR) is briefly described, bearing in mind its application to amorphous semiconductors. The ODMR measurements including those which are time-resolved are reviewed on amorphous semiconductors, particularly on hydrogenated amorphous silicon (a-Si: H). The nature of the recombination centres in a-Si: H is also discussed.

§1. Introduction

The recombination processes and the nature of recombination centres in amorphous semiconductors have attracted much interest from viewpoints of the fundamental understanding of the band tail and gap states and also the application, such as solar cells and imaging devices. The technique of optically detected magnetic resonance[1] (ODMR) provides useful information about these problems because it links ESR and luminescence by monitoring the change in luminescence intensity at resonance. The nature of recombination centres and the radiative and nonradiative recombination processes involved in the luminescence can thus be investigated from microscopic viewpoints. In this paper we review briefly the principle of ODMR in amorphous semiconductors which is based on spin-dependent recombination processes and also the ODMR experiments which have been reported so far, particularly those on hydrogenated amorphous silicon (a-Si: H). The time-resolved ODMR measurements are also reviewed for a-Si: H, and the nature of recombination centres in a-Si: H is discussed on the basis of the ODMR results.

§2. Spin-Dependent Recombination—Principle of Optically Detected Magnetic Resonance

Spin-dependent recombination processes, either radiative or nonradiative, give a basis for ODMR measurement.[2-8] In amorphous semiconductors, one usually monitors the luminescence intensity to observe ODMR signals as a variation at resonance. If emitting states have a certain anisotropic symmetry and emitted light is thus polarized, however, it would be useful to observe ODMR signals by monitoring the polarization of this light to assess the symmetry of the recombination centres and examine the spin-memory effect. In this section, this is undertaken for triplet exciton recombination. In the case of electron-hole pair recombination, we consider only the case in which ODMR signals are detected while monitoring the luminescence intensity, because any polarization effect would be obliterated by structural disorder of amorphous materials or cancelled out by random distribution of electron-hole pairs in separation and orientation. In the following, we deal with the trapped electron-hole pair recombination for cases with and without spin memory effect in §2.1 and the triplet exciton recombination in §2.2.

2.1 *Trapped electron-hole pair recombination*

2.1.1 *Without spin memory effect*

First, we deal with the radiative electron-hole pairs.[8] We suppose that after optical excitation the created electrons and holes immediately lose their spin memory and are trapped by electron centres and hole centres, respectively, with random spin orientation. The electron-hole pairs are then generated at an equal rate among four Zeeman levels in the presence of a magnetic field, as shown in Fig. 1, i.e., $G[N-(n_1+n_2+n_3+n_4)]$, where G and N designate the generation rate and the total number of pairs of electron and hole traps, respectively, and n_1, n_2, n_3 and n_4 refer to the population of each level. In Fig. 1, R and R^* are the recombination rates of the singlet configuration states, n_2 and n_3, and of the triplet configuration states, n_1 and n_4, respectively. R is the sum of the radiative and nonradiative recombination rates, while R^* is mostly the nonradiative recombination rate. The rate equations describing the time-variation of n_1, n_2, n_3 and n_4 are given by

$$\frac{dn_1}{dt} = G[N-(n_1+n_2+n_3+n_4)] - R^* n_1 - \frac{1}{T_1} n_1 + \frac{(n_1+n_2+n_3+n_4)\, e^{-E_1/kT}}{T_1(e^{-E_1/kT}+e^{-E_2/kT}+e^{E_2/kT}+e^{E_1/kT})} + W_h(n_3-n_1) + W_e(n_2-n_1),$$

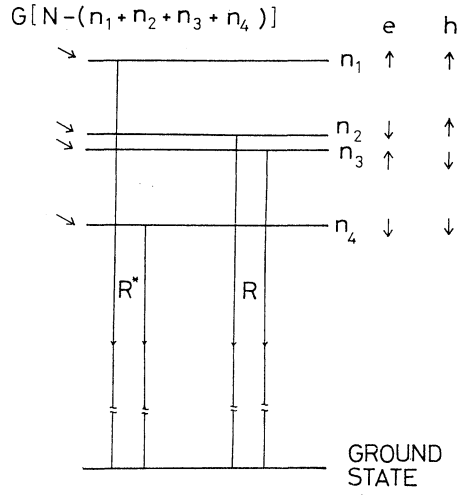

Fig. 1. Zeeman levels of an electron-hole pair in the presence of magnetic field. See the text for symbols used in the figure.[8]

$$\frac{dn_2}{dt}=G[N-(n_1+n_2+n_3+n_4)]-Rn_2-\frac{1}{T_1}n_2+\frac{(n_1+n_2+n_3+n_4)\,e^{-E_2/kT}}{T_1(e^{-E_1/kT}+e^{-E_2/kT}+e^{E_2/kT}+e^{E_1/kT})}+W_h(n_4-n_2)+W_e(n_1-n_2),$$

$$\frac{dn_3}{dt}=G[N-(n_1+n_2+n_3+n_4)]-Rn_3-\frac{1}{T_1}n_3+\frac{(n_1+n_2+n_3+n_4)\,e^{E_2/kT}}{T_1(e^{-E_1/kT}+e^{-E_2/kT}+e^{E_2/kT}+e^{E_1/kT})}+W_h(n_1-n_3)+W_e(n_4-n_3),$$

$$\frac{dn_4}{dt}=G[N-(n_1+n_2+n_3+n_4)]-R^*n_4-\frac{1}{T_1}n_4+\frac{(n_1+n_2+n_3+n_4)\,e^{E_1/kT}}{T_1(e^{-E_1/kT}+e^{-E_2/kT}+e^{E_2/kT}+e^{E_1/kT})}W_h(n_2-n_4)+W_e(n_3-n_4), \quad (1)$$

where T_1 is the spin-lattice relaxation time of each Zeeman level, assuming the same relaxation times, E_1 and E_2 are given by $[(g_h+g_e)/2]\mu_B H$ and $[(g_h-g_e)/2]\mu_B H$, respectively, using g-values of the trapped electron, g_e, and trapped hole, g_h, Bohr magneton, μ_B, and magnetic field, H, and W_e and W_h are the ESR transition rates of trapped electrons and holes, respectively. In eq. (1), each term of r.h.s. of each equation designates the generation term, the recombination term, the relaxation term, the thermalization term, the ESR transition term of holes and the ESR transition term of electrons, respectively. Since the luminescence intensity is proportional to (n_2+n_3), its relative change at resonance is easily obtained from eq. (1) in the steady-state condition as follows:

$$(\Delta I/I)_{ESR}=\frac{(R^*+4G)\{(R-R^*)+(2/T_1)[(1-x_e)(1-x_h)/(1+x_e)(1+x_h)]\}}{(R+R^*+8G)\{R^*+(2/T_1)[(x_e+x_h)/(1+x_e)(1+x_h)]\}}\,\frac{2T_1^*W}{1+2T_1^*W}, \quad (2)$$

$$\frac{1}{T_1^*}=2\frac{RR^*+2G(R+R^*+(2/T_1))+(1/T_1)[1/(1+x_e)(1+x_h)][R^*(1+x_ex_h)+R(x_e+x_h)]}{R+R^*+8G}, \quad (3)$$

$$x_e=e^{-g_e\mu_B H/kT},\qquad x_h=e^{-g_h\mu_B H/kT}, \quad (4)$$

where T_1^* is the effective spin-lattice relaxation time, and W is either W_e or W_h, depending on the resonances of trapped electrons or holes. $(\Delta I/I)_{ESR}$ given by eq. (2) is approximated in the following conditions:

(I) Unthermalized case (R, $R^*\gg 1/T_1$)

(i) For a small value of G,

$$(\Delta I/I)_{ESR}\cong\frac{R-R^*}{R+R^*}\,\frac{2T_1^*W}{1+2T_1^*W}, \quad (5)$$

$$1/T_1^*\cong 2\left(R^*+(1/T_1)\frac{x_e+x_h}{(1+x_e)(1+x_h)}+2G\right). \quad (6)$$

(ii) For a large value of G,

$$(\Delta I/I)_{ESR}\cong\frac{R-R^*}{2R^*}\,\frac{2T_1^*W}{1+2T_1^*W}, \quad (7)$$

$$1/T_1^*\cong R/2. \quad (8)$$

(II) Thermalized case (R, $R^*\ll 1/T_1$)

$$(\Delta I/I)_{ESR}\cong\frac{R^*+4G}{R+R^*+8G}\,\frac{(1-x_e)(1-x_h)}{x_e+x_h}\,\frac{2T_1^*W}{1+2T_1^*W}, \quad (9)$$

The above results of $(\Delta I/I)_{ESR}$ in eqs. (5)–(9) are easily interpreted as follows: When R is greater than R^* for the unthermalized case, a large increase in the luminescence intensity at resonance is expected from eqs. (5) and (7); namely, following the above conditions, n_2 and n_3 become smaller than n_1 and n_4 in the steady state, so that when ESR of electrons occurs between n_1 and n_2 and also between n_3 and n_4, n_2 and n_3 become large and, as a result, the luminescence intensity increases compared to that before ESR occurs. A similar situation also occurs for ESR of holes. The above results have already been shown by Kaplan *et al.*[5] and Dunstan and Davies.[6]

For the thermalized case, i.e., when the spin-lattice relaxation rate, $1/T_1$, is greater than R and R^*, the obtained $(\Delta I/I)_{ESR}$ is expected to be smaller than that for the unthermalized case. This is quite reasonable, because thermalization among the four Zeeman levels tends to eliminate a great difference in populations between n_1 (or n_4) and n_2 (or n_3) which has been realized from rapid radiative recombination.

Secondly, we consider the nonradiative recombination[8] which occurs, for example, between electrons at the radiative centres and holes at the nonradiative centres such as dangling bond centres in a-Si: H. Such nonradiative recombination process is shown for the case of a-Si: H in Fig. 2. Here, recombination between an electron and a hole is considered in a similar way to the radiative trapped electron-hole pairs illustrated in Fig. 1, although the recombination in the present case is nonradiative. Thus, instead of an enhancement of radiative recombination at resonance, i.e., the results given by eqs. (2)–(9), ESR of either electrons or holes in the present case gives rise to an enhancement of nonradiative recombination, i.e., a decrease in the luminescence intensity. Here we

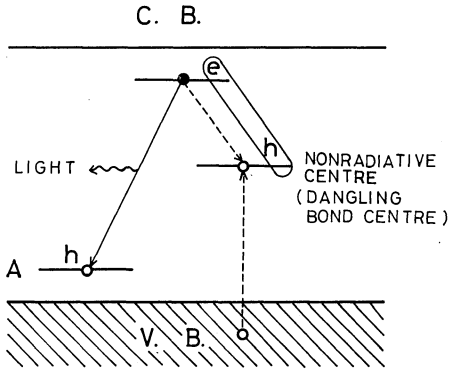

Fig. 2. Schematic diagram of radiative and nonradiative recombination processes. Solid and dashed arrows show radiative and nonradiative recombination, respectively. A radiative hole centre is the A centre.[8]

present the relative change in luminescence intensity at resonance of either the nonradiative centre or the radiative trapped electron for the unthermalized case:

$$(\Delta I/I)_{\mathrm{ESR}} = -\frac{R_{\mathrm{ns}}^2}{(2R_l+R_{\mathrm{ns}})(8G+2R_l+R_{\mathrm{ns}})}\frac{2T_1^*W}{1+2T_1^*W}, \quad (10)$$

$$1/T_1^* = \frac{4G(2R_l+R_{\mathrm{ns}})+2R_l(R_l+R_{\mathrm{ns}})}{8G+2R_l+R_{\mathrm{ns}}}, \quad (11)$$

where W is the ESR transition rate of either the nonradiative centre or the radiative trapped electron, and R_l and R_{ns} designate the radiative recombination rate and the nonradiative recombination rate (for the singlet configuration of a radiative electron-nonradiative hole pair), respectively. We neglect the nonradiative recombination rate for the triplet configuration. As shown by eqs. (10) and (11), $(\Delta I/I)_{\mathrm{ESR}}$ is negative in accordance with the expectation mentioned above.

The generation rate, G, in eq. (1) is not directly connected to the excitation power. Thus we consider this problem in Appendix A, where a relationship between G and the generation rate of free electron-hole pairs that is directly connected to the excitation power is given as well as the relationship between luminescence intensity and G.

2.1.2 *With spin-memory effect*

We assume that free electrons and holes have spin memory after being excited into the conduction band and valence band, respectively. They are captured by charged centres, i.e., electron traps or hole traps; consequently, the generation rate depends upon the spin states of trapped electron-hole pairs. We consider the case of weak excitation and neglect the saturation effect for the trapping of electrons and holes. Then, taking into account the spin memory effect, the rate equations for n_1, n_2, n_3 and n_4 are given by[9]

$$\frac{dn_1}{dt} = \frac{1}{2}\varepsilon G - R^*n_1 - \frac{1}{T_1}n_1 + \frac{(n_1+n_2+n_3+n_4)\,e^{-E_1/kT}}{T_1(e^{-E_1/kT}+e^{-E_2/kT}+e^{E_2/kT}+e^{E_1/kT})} + W_{\mathrm{h}}(n_3-n_1)+W_{\mathrm{e}}(n_2-n_1),$$

$$\frac{dn_2}{dt} = \frac{1}{2}(1-\varepsilon)G - Rn_2 - \frac{1}{T_1}n_2 + \frac{(n_1+n_2+n_3+n_4)\,e^{-E_2/kT}}{T_1(e^{-E_1/kT}+e^{-E_2/kT}+e^{E_2/kT}+e^{E_1/kT})} + W_{\mathrm{h}}(n_4-n_2)+W_{\mathrm{e}}(n_1-n_2),$$

$$\frac{dn_3}{dt} = \frac{1}{2}(1-\varepsilon)G - Rn_3 - \frac{1}{T_1}n_3 + \frac{(n_1+n_2+n_3+n_4)\,e^{E_2/kT}}{T_1(e^{-E_1/kT}+e^{-E_2/kT}+e^{E_2/kT}+e^{E_1/kT})} + W_{\mathrm{h}}(n_1-n_3)+W_{\mathrm{e}}(n_4-n_3),$$

$$\frac{dn_4}{dt} = \frac{1}{2}\varepsilon G - R^*n_4 - \frac{1}{T_1}n_4 + \frac{(n_1+n_2+n_3+n_4)\,e^{E_1/kT}}{T_1(e^{-E_1/kT}+e^{-E_2/kT}+e^{E_2/kT}+e^{E_1/kT})} + W_{\mathrm{h}}(n_2-n_4)+W_{\mathrm{e}}(n_3-n_4), \quad (12)$$

where ε is the measure of the spin memory loss and the definitions of other parameters are the same as in eq. (1) except for G which corresponds to GN in eq. (1).

Since the luminescence intensity is proportional to (n_2+n_3), the relative change in this intensity at resonance is easily obtained from eq. (12) in the steady-state condition as follows;

$$(\Delta I/I)_{\mathrm{ESR}} = \frac{R^*[\varepsilon R+(\varepsilon-1)R^*+(1/T_1)[(1-x_{\mathrm{e}})(1-x_{\mathrm{h}})/(1+x_{\mathrm{e}})(1+x_{\mathrm{h}})]]}{(R+R^*)[(1-\varepsilon)R^*+(1/T_1)[(x_{\mathrm{e}}+x_{\mathrm{h}})/(1+x_{\mathrm{e}})(1+x_{\mathrm{h}})]]}\frac{2T_1^*W}{1+2T_1^*W}, \quad (13)$$

$$\frac{1}{T_1^*} = 2\frac{RR^*+(1/T_1)(1/(1+x_{\mathrm{e}})(1+x_{\mathrm{h}}))[R^*(1+x_{\mathrm{e}}x_{\mathrm{h}})+R(x_{\mathrm{e}}+x_{\mathrm{h}})]}{R+R^*}, \quad (14)$$

$$x_{\mathrm{e}} = e^{-g_{\mathrm{e}}\mu_{\mathrm{B}}H/kT}, \qquad x_{\mathrm{h}} = e^{-g_{\mathrm{h}}\mu_{\mathrm{B}}H/kT}, \quad (15)$$

where T_1^* is the effective spin-lattice relaxation time, and W is either W_{e} or W_{h}, depending on the resonances of either trapped electrons or holes.

In the extreme case of $\varepsilon=0$ (complete spin memory), the following result is obtained;

$$(\Delta I/I)_{\mathrm{ESR}} = -\frac{R^*[R^*-(1/T_1)[(1-x_{\mathrm{e}})(1-x_{\mathrm{h}})/(1+x_{\mathrm{e}})(1+x_{\mathrm{h}})]]}{(R+R^*)[R^*+(1/T_1)[(x_{\mathrm{e}}+x_{\mathrm{h}})/(1+x_{\mathrm{e}})(1+x_{\mathrm{h}})]]} \times \frac{2T_1^*W}{1+2T_1^*W}, \quad (16)$$

where T_1^* is given by eq. (14). It is noted that T_1^* does not depend on ε. If R^* is greater than $(1/T_1)[(1-x_{\mathrm{e}})(1-x_{\mathrm{h}})/(1+x_{\mathrm{e}})(1+x_{\mathrm{h}})]$, $(\Delta I/I)_{\mathrm{ESR}}$ becomes negative.

For unthermalized trapped electron-hole pairs, $(\Delta I/I)_{\mathrm{ESR}}$ is simply expressed by

$$(\Delta I/I)_{\mathrm{ESR}} = \frac{\varepsilon R+(\varepsilon-1)R^*}{(1-\varepsilon)(R+R^*)}\frac{2T_1^*W}{1+2T_1^*W}, \quad (17)$$

$$\frac{1}{T_1^*} = \frac{2RR^*}{R+R^*}, \quad (18)$$

Thus the luminescence intensity increases or decreases at resonance, depending on the spin memory degree, in contrast to the case of eqs. (5) and (7) in which the intensity always increases at resonance.

2.2 *Triplet exciton recombination*

Since the first observation[10] of triplet exciton resonance in semiconductors using the ODMR technique, a number of investigations have been reported in crystalline semiconductors.[1,11] Very recently triplet exciton resonance has also been observed in amorphous semiconductors such as chalcogenide glasses[12-14] and amorphous phosphorus.[15,16] The following model using the rate equations was originally applied to crystalline semiconductors such as GaSe,[10] but is also applicable to amorphous semiconductors.

The Zeeman levels of triplet excitons, $S=1$, are shown in Fig. 3(a) and (b) in the presence of a crystalline field of axial symmetry and a magnetic field. The generation rates and recombination rates for these levels, $S_z=+1, 0, -1$, are designated as G_1, G_2 and G_3, and R_1, R_2 and R_3,

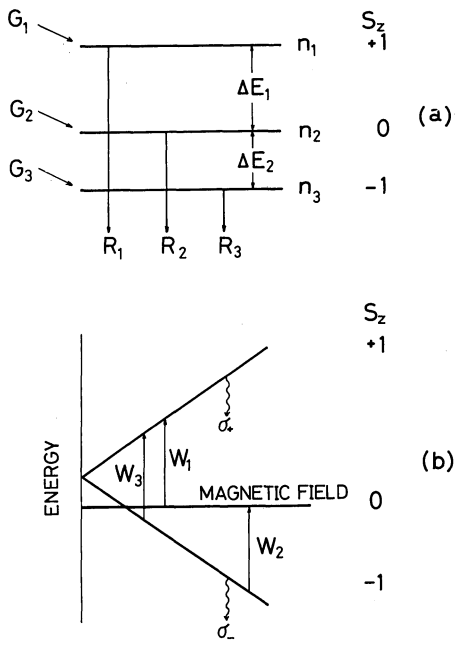

Fig. 3. Zeeman levels of a triplet exciton in the presence of magnetic field. (a): For a given magnetic field. (b): As a function of magnetic field whose direction is parallel to the symmetry axis of the centre. W_1 and W_2 are the transitions for $S_z=\pm1$, while W_3 is that for $S_z=\pm2$. See text for symbols used in the figure.

respectively. The separations between the $S_z=+1$ level and the $S_z=0$ level and between the $S_z=0$ level and the $S_z=-1$ level are ΔE_1 and ΔE_2, respectively. The rate equations for the populations of each level, n_1, n_2 and n_3 are given by

$$\frac{dn_1}{dt}=G_1-R_1n_1-\frac{1}{T_1}n_1+\frac{(n_1+n_2+n_3)\,e^{-\Delta E_1/kT}}{T_1(1+e^{-\Delta E_1/kT}+e^{\Delta E_2/kT})}+W_1(n_2-n_1),$$

$$\frac{dn_2}{dt}=G_2-R_2n_2-\frac{1}{T_1}n_2+\frac{(n_1+n_2+n_3)}{T_1(1+e^{-\Delta E_1/kT}+e^{\Delta E_2/kT})}+W_1(n_1-n_2)+W_2(n_3-n_2),$$

$$\frac{dn_3}{dt}=G_3-R_3n_3-\frac{1}{T_1}n_3+\frac{(n_1+n_2+n_3)\,e^{\Delta E_2/kT}}{T_1(1+e^{-\Delta E_1/kT}+e^{\Delta E_2/kT})}+W_2(n_2-n_3), \tag{19}$$

where W_1 and W_2 are the rates of ESR transitions as shown in Fig. 3(b). Solving these equations in the steady state condition, n_1 and n_3 are exactly obtained, as shown in Appendix. Here we present the calculated results for unthermalized cases under two conditions, i.e., R_1, $R_3\gg R_2\gg 1/T_1$ and R_1, $R_3\gg 1/T_1\gg R_2$.

We deal with the emissions from the $S_z=+1$ and $S_z=-1$ levels which are circularly polarized and designated as σ_+ and σ_- emissions, respectively. As seen in Fig. 3(b), two resonances generally occur under application of microwave radiation, scanning magnetic field, which are referred to as low field and high field resonance. The intensities of σ_+ and σ_- emissions are proportional to n_1 and n_3, respectively. Monitoring these emission intensities, the ODMR is observed as a variation at resonances W_1 and W_2, $(\Delta I/I)_{ESR}$ as follows:

(I) R_1, $R_3\gg R_2\gg 1/T_1$

(i) σ_- emission

$W_2\neq0$, $W_1=0$

(high field resonance)

$$(\Delta I/I)_{ESR}\cong\frac{G_2R_3-G_3R_2}{G_3R_3}\frac{2T_1^*W_2}{1+2T_1^*W_2}, \tag{20}$$

$$1/T_1^*\cong 2R_2, \tag{21}$$

(ii) σ_+ emission

$W_1\neq0$, $W_2=0$

(low field resonance)

$$(\Delta I/I)_{ESR}\cong\frac{G_2R_1-G_1R_2}{G_1R_1}\frac{2T_1^*W_1}{1+2T_1^*W_1}, \tag{22}$$

$$1/T_1^*\cong 2R_2, \tag{23}$$

(iii) σ_- emission

$W_1\neq0$, $W_2=0$

(low field resonance)

$$(\Delta I/I)_{ESR}\cong\frac{(2G_1R_2-G_2R_1)a\,e^{\Delta E_2/kT}}{R_1(G_3R_2+G_2ae^{\Delta E_2/kT})}\frac{2T_1^*W_1}{1+2T_1^*W_1}, \tag{24}$$

$$1/T_1^*\cong 2R_2, \tag{25}$$

a in eq. (24) is given by eq. (B·7) in Appendix B.

(iv) σ_+ emission

$W_2\neq0$, $W_1=0$

(high field resonance)

$$(\Delta I/I)_{ESR}\cong-\frac{(G_1a+R_1G_2)a\,e^{-\Delta E_1/kT}}{R_1(R_2G_1+G_2a\,e^{-\Delta E_1/kT})}\frac{2T_1^*W_2}{1+2T_1^*W_2}, \tag{26}$$

$$1/T_1^*\cong 2R_2, \tag{27}$$

(II) R_1, $R_3\gg 1/T_1\gg R_2$

(i) σ_- emission

$W_2\neq0$, $W_1=0$

(high field resonance)

$$(\Delta I/I)_{ESR}\cong\frac{G_2\left[\frac{1}{T_1}-a(1+e^{\Delta E_2/kT})\right]}{G_3\left(\frac{1}{T_1}-a\right)+G_2a\,e^{\Delta E_2/kT}}\frac{2T_1^*W_2}{1+2T_1^*W_2}, \tag{28}$$

$$1/T_1^*\cong 2\left(\frac{1}{T_1}-a\right), \tag{29}$$

(ii) σ_+ emission

$W_1\neq0$, $W_2=0$

(low field resonance)

$$(\Delta I/I)_{ESR}\cong\frac{G_2\left[\frac{1}{T_1}-a(1+e^{-\Delta E_1/kT})\right]}{G_1\left(\frac{1}{T_1}-a\right)+G_2a\,e^{-\Delta E_1/kT}}\frac{2T_1^*W_1}{1+2T_1^*W_1}, \tag{30}$$

$$1/T_1^*\cong 2\left(\frac{1}{T_1}-a\right), \tag{31}$$

(iii) σ_- emission

$W_1\neq0$, $W_2=0$

(low field resonance)

$$(\Delta I/I)_{ESR}\cong-\frac{G_2a\,e^{\Delta E_2/kT}}{G_3\left(\frac{1}{T_1}-a\right)+G_2a\,e^{\Delta E_2/kT}}\frac{2T_1^*W_1}{1+2T_1^*W_1}, \tag{32}$$

$$1/T_1^* \cong 2\left(\frac{1}{T_1}-a\right), \tag{33}$$

(iv) σ_+ emission

$W_2 \neq 0, \quad W_1 = 0$

(high field resonance)

$$(\Delta I/I)_{\mathrm{ESR}} \cong -\frac{G_2 a\, \mathrm{e}^{-\Delta E_1/kT}}{G_1\left(\frac{1}{T_1}-a\right)+G_2 a\, \mathrm{e}^{-\Delta E_1/kT}} \frac{2T_1^* W_2}{1+2T_1^* W_2}, \tag{34}$$

$$1/T_1^* \cong 2\left(\frac{1}{T_1}-a\right), \tag{35}$$

We note here some interesting results derived from eqs. (20)–(35). For case (I), when the generation rates for three levels are equal, i.e., $G_1=G_2=G_3$, the high field resonance and the low field resonance give rise to an increase in the intensities of σ_- and σ_+ emissions, respectively. This is quite similar to the case which we considered in §2.1. On the other hand, when σ_- and σ_+ emissions are monitored to observe low field and high field resonance, respectively, the thermalized effect between the $S_z=0$ and $S_z=-1$ levels and between the $S_z=+1$ and $S_z=0$ levels plays an important role in observing those respective resonances.

Since electron-hole pairs with singlet states are optically excited, the generation rates would be greater for the $S_z=0$ state than for the $S_z=\pm 1$ states within a finite period determined by the spin memory time, i.e., $G_2 \gg G_1$ and G_3. Then, following eqs. (20) and (22), a large increase in the intensities of the σ_- and σ_+ emissions would be expected at the high field and low field resonances, respectively. This is again in contrast to the case of radiative electron-hole pairs with spin memory in which the $S_z=0$ state (antiparallel electron and hole spins) is the emitting state, so that the luminescence intensity decreases at resonance, as shown in §2.1.2.

In the above consideration, we dealt with two circularly polarized emissions from $S_z=+1$ and $S_z=-1$ levels. This is a special case wherein the luminescence is monitored along a magnetic field whose direction coincides with the symmetry axis of a centre to which an exciton is bound. In general, the $S_z=0$ level is also an emitting level. The above calculation is easily extended to this case and since essentially this type of emission corresponds to the case of radiative electron-hole pairs considered in §2.1, the sign of the observed change in luminescence intensity at resonance depends on the magnitudes of G_1, G_2 and G_3, i.e., $\Delta I<0$ for $G_2 \gg G_1$ and G_3, and otherwise, $\Delta I>0$.

In amorphous semiconductors, the symmetry axis of the triplet exciton state is, in general, randomly oriented, so that it seems difficult to observe ODMR signals by monitoring the circular polarization of emitted light, but some favorable cases will be discussed in §3.

In the following, we briefly mention a case which monitors the intensity of emitted light, a usual case for ODMR of amorphous semiconductors. Here, the change in luminescence intensity at resonance is generally given by

$$(\Delta I/I)_{\mathrm{ESR}} = \frac{\tilde{R}_1 \Delta n_1 + \tilde{R}_2 \Delta n_2 + \tilde{R}_3 \Delta n_3}{\tilde{R}_1 n_1 + \tilde{R}_2 n_2 + \tilde{R}_3 n_3}, \tag{36}$$

when $\tilde{R}_1$, $\tilde{R}_2$ and $\tilde{R}_3$ designate the radiative part of respective recombination rates. In eq. (36), we assume that the level splitting as shown in Fig. 3 is not resolved in the emission spectrum. This is the usual case for ODMR experiments, because the level splitting is small compared to the resolution of emitted light.

§3. General Aspects of ODMR Measurements in Amorphous Semiconductors

In this section we briefly review general aspects of the ODMR measurements in amorphous semiconductors which have been reported so far. Since ODMR measurements in a-Si: H were carried out independently by Morigaki *et al.*,[17-20] Biegelsen *et al.*[21] and Lampel *et al.*,[22] a number of investigations have been reported on a-Si: H and a few papers have been published on chalcogenide glasses[12-14] and nictide amorphous semiconductors.[15,16] In this section, we concentrate on ODMR of the latter two categories; ODMR of a-Si: H will be discussed in §4.

Triplet exciton resonance in amorphous semiconductors was observed for the first time by Depinna and Cavenett[15] in a-P and recently it has also been observed in a-As_2S_3[12,14] and a-As_2Se_3.[13] Figure 4 shows the ODMR spectrum observed by Depinna and Cavenett.[15] Since similar triplet exciton resonance spectra have been observed in c-As_2S_3[14] and c-As_2Se_3,[13] it is speculated that similar recombination centres are involved in both these amorphous and crystalline materials. Depinna and Cavenett[12,13] have proposed that the exciton bound to IVAP (intimate valence alternation pairs)[35] is a candidate for possible recombination centres in a-As_2S_3 and a-As_2Se_3. In these amorphous semiconductors, two ESR transitions expected for the triplet excitons, i.e., W_1 and W_2 in Fig. 3(b), are not generally resolved and the separation between them is averaged out for random orientation of the z-axis. Furthermore, the $S_z=\pm 2$ transition has been observed in a-As_2S_3,[12,14] a-As_2Se_3[13] and a-P,[15] as shown in Fig. 4 for a-P. Thus, in amorphous semiconductors, ODMR of triplet excitons appears not to be observed as a change in the circular polarization. However, if one uses the time-resolved ODMR technique there is

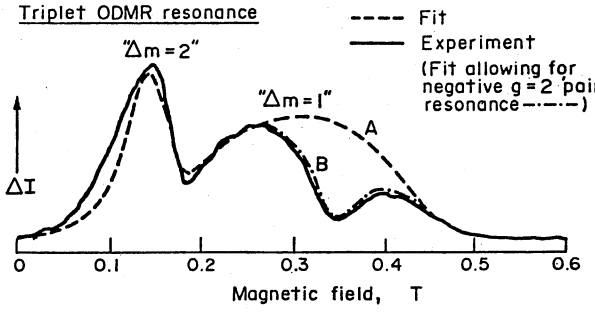

Fig. 4. ODMR spectrum of triplet excitons in a-P. Dashed line A is a fit of the triplet resonance including $S_z=\pm 1$ and $S_z=\pm 2$ transitions, using appropriate values of the parameter. Dashed line B includes a negative contribution from the pair resonance. (after Depinna and Cavenett[15]).

the possibility that emitted light from triplet excitons may be circularly polarized for a short time after pulsed excitation and thus ODMR might be observed as a change in the intensities of σ_+ and σ_- emissions. For As_2S_3, it has been found that when the sample is excited by linearly polarized light, the fast decay luminescence with a decay time of 10 ns has a polarization memory.[36] Localized excitons have been considered as possible candidates for recombination centres. The amorphous As_2S_3 structure has been thought to consist of AsS_3 pyramids. From this picture of the amorphous structure, it is speculated that the recombination centres are excitons either bound to AsS_3 pyramids or to IVAP. An AsS_3 unit has axial symmetry whose axis is along the direction from the centre of the plane including three S atoms towards the As site. Thus, if the state of the triplet exciton being localized at this unit has mainly axial symmetry, the above possibility to observe ODMR of triplet excitons through circular (or linear) polarization may be applied.

The electron-hole pair recombination gives rise to the observation of electron resonance and hole resonance by monitoring the luminescence intensity. This is the case of ODMR of distant electron-hole pairs which has been observed in a-As_2S_3,[12,14,36,41] a-As_2Se_3,[13,37] a-P,[15] a-Si: H[8,17-34] and a-Si: H, F.[25] In chalcogenide glasses[38-40] except for a-GeS_2,[59] no ESR is observed in the dark, but light-induced ESR is observed under continuous excitation. The light-induced ESR signal in general consists of electron and hole resonance. Isolated defects[42] such as D^+ and D^- capture electrons and holes, respectively, and then give rise to light-induced resonance.[38] The connection between these resonances and ODMR of distant electron-hole pairs is not clear. Deppina and Cavenett[12,13] have suggested that ODMR of distant electron-hole pairs may be due to either an electron or a hole bound to IVAP, whereas Biegelsen and Street[40] have suggested that light-induced ESR centres associated with luminescence fatigue are IVAPs capturing either an electron or a hole. Further investigations are clearly necessary to reach a definite conclusion on the defect centres responsible for light-induced ESR and ODMR in chalcogenide glasses.

§4. ODMR Measurements in a-Si: H and a-Si: H, F

Luminescence of a-Si: H[43] has been considered due to radiative recombination of trapped electron-hole pairs. The band tail states and the gap states act as trapping centres and/or recombination centres. No evidence of exciton recombination has been found for luminescence in a-Si: H. ODMR results are analysed in terms of the distant electron-hole pairs described in §2.1. The ODMR spectra consist of three components which are designated as the D_1, D_2 and A lines. The D_1 and D_2 lines are not generally resolved because of the overlap of the A line (see Fig. 5(a), (b)). Figure 6 shows a typical recording trace of the ODMR spectra observed by monitoring the luminescence intensity at various luminescence energies for a sample of a-Si: H (No. 519) prepared by glow-discharge decomposition of silane gas at a deposition temperature of 300°C.[24] The D_1 and D_2 lines are the quenching signals for luminescence with g-values of 2.018 and

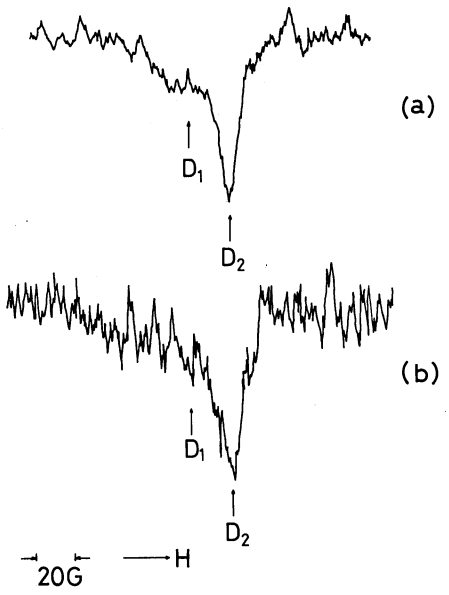

Fig. 5. D_1 and D_2 lines observed at 10 GHz and 2 K, monitoring the intensity of emitted light of 1.54 eV for (a) and 1.50 eV for (b) under excitation by unfocused argon ion laser light of 25 mW at 514.5 nm. (a): a-Si: H sample No. 524 (T_s=200°C) (taken after prolonged laser light irradiation),[24] (b): a-Si: H, F No. 814 (T_s=300°C).[26]

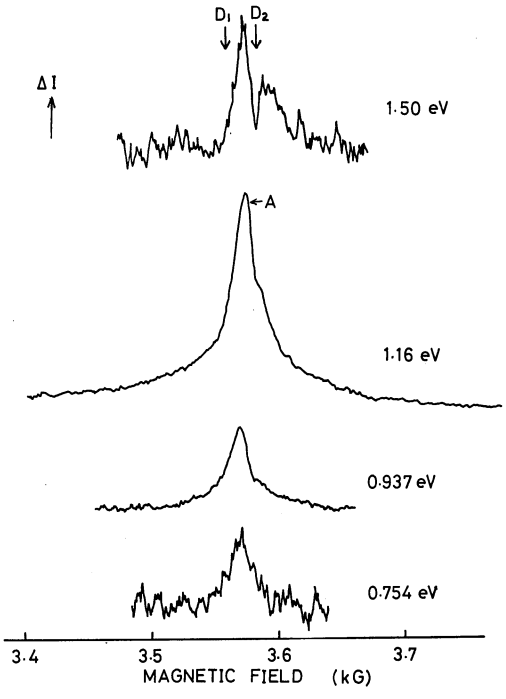

Fig. 6. ODMR spectra observed at 10 GHz and 2 K in a-Si: H No. 519 (T_s=300°C), monitoring the intensity of emitted light whose photon energy is indicated in the figure, under excitation by unfocused argon ion laser light of 25 mW at 514.5 nm.[24]

2.006, respectively and thus are attributed to nonradiative centres, according to the theoretical consideration given in §2.1. The g-value of the D_2 line coincides with that of dangling bond centres in a-Si, i.e., 2.0055,[44] so that the D_2 centre is identified as being due to a dangling bond centre; the nature of the D_1 centre, however, is not clear but will be discussed in §6. The A line appears as an enhancing signal for the luminescence and its g-value depends on luminescence energy and microwave power.[8,23] According to the theoretical consideration given in §2.1,

the resonance may be due to either electrons or holes of radiative electron-hole pairs. From several reasons we have concluded that the A line is due to trapped holes which are weakly coupled with trapped electrons;[23] the positive g-shift of the A line suggests that the line is due to holes; the variation of g-value and linewidth with luminescence energy and microwave power is reasonably interpreted in terms of such weak interaction between trapped electrons and holes. Here we assume that electron traps are distributed over a certain range of conduction band tail, so that their g-values are spread. The extent of the g-value of trapped electrons broadens their ODMR signal, so that ODMR signals of trapped electrons are difficult to be observed. Also, trapped electrons presumably contribute to both an increase and a decrease in the luminescence intensity at resonance, according to the consideration given in §2.1, and such a two-fold effect tends to cancel out a change in luminescence intensity at electron resonance. The above model can also be used to interpret the inhomogeneous broadening of the A line which is demonstrated by a striking difference in linewidth between two microwave frequencies, as shown in Fig. 7. When the luminescence intensity was monitored at 1.16 eV, the full widths of half amplitude were 38 G and 92 G at 10 GHz and 34 GHz, respectively (see Figs. 6 and 7).

The ODMR of D_1, D_2 and A centres observed at 2 K has been considered to correspond to the unthermalized case given in §2.1.1.[8] The spin memory effect is neglected in the steady state ODMR of a-Si: H.

The spectral dependences of ODMR signals enable us to elucidate the recombination processes involved in the luminescence. A typical example of the spectral dependence of $(\Delta I/I)_{ESR}$ is shown in Fig. 8 as well as the luminescence spectrum for a sample of a-Si: H (No. 519). In this figure, cases of both before and after luminescence fatigue are shown, in which the fatigue[45-47] is brought about by prolonged light irradiation, *e.g.*, exposure to laser light of 360 mW at 514.5 nm for 30 min at 2 K (total photon number: 2.4×10^{22} cm^{-2}). The spectral dependence of ODMR signals may be interpreted by the results given in §2.1. Details of the analysis are given in refs. 23–26 and the level scheme such as is shown in Fig. 9 is derived from such analysis. This figure shows a schematic diagram of the recombination processes and the level of recombination centres. Details are given in refs. 26 and 28 for samples of a-Si: H and a-Si: H, F prepared under various conditions.

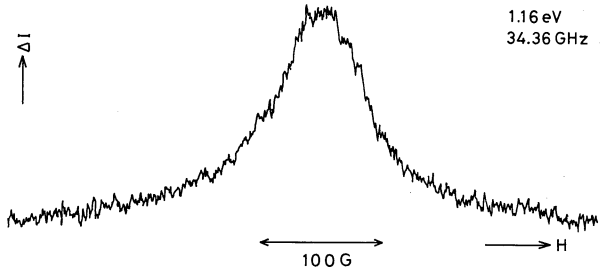

Fig. 7. ODMR spectrum observed at 34 GHz and 2 K in a-Si: H No. 12 (T_s=300 °C), monitoring emitted light of 1.16 eV under excitation by argon ion laser light of 200 mW at 514.5 nm.[28]

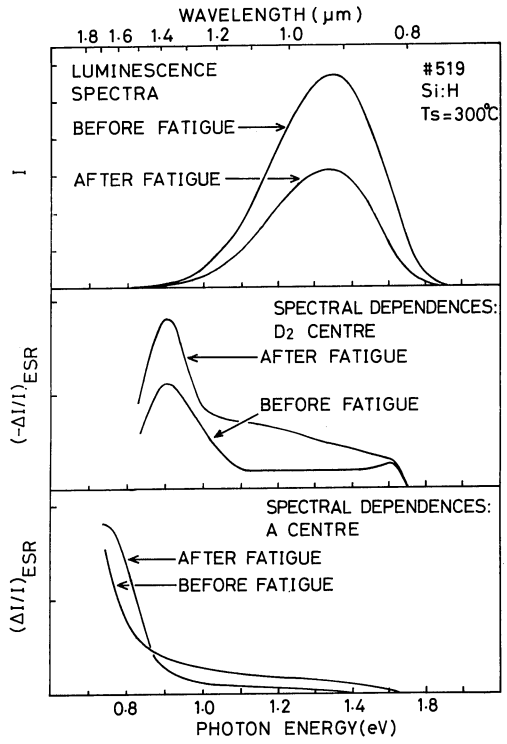

Fig. 8. Luminescence spectrum and spectral dependences of $(\Delta I/I)_{ESR}$ at resonances of the D_2 and A centres at 2 K in a-Si: H No. 519 (T_s=300 °C). Each value in the coordinates is plotted in arbitrary units.[24]

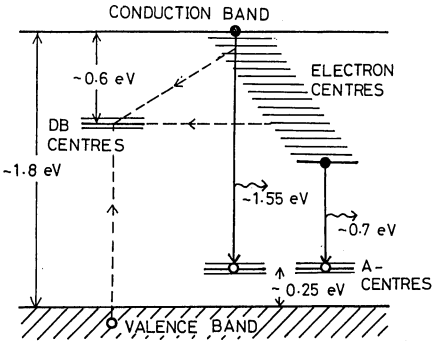

Fig. 9. Schematic diagram of radiative and nonradiative recombination processes which are indicated by solid and dashed lines, respectively. Energies relevant to the positions of the localized levels are shown for a-Si: H No. 12. DB centres are doubly occupied dangling bond centres.[23,24]

The nature of the recombination centres observed by the ODMR measurements will be discussed in §6.

Before proceeding to the next section, we would like to mention briefly the ODMR results associated with prolonged light irradiation. Figure 8 shows an increase of the absolute magnitude of $(\Delta I/I)_{ESR}$ at the dangling bond resonance such as that observed after prolonged light irradiation, and clearly indicates that dangling bond centres are created by prolonged irradiation. The details have been reported in ref. 24.

§5. Time-Resolved ODMR in a-Si: H

The time-resolved ODMR (TRODMR) measurements provide important information about the dynamical behaviour of recombination processes.[48,49] The first TRODMR measurements on a-Si: H were done by Morigaki *et al.*[18] and will be discussed together with

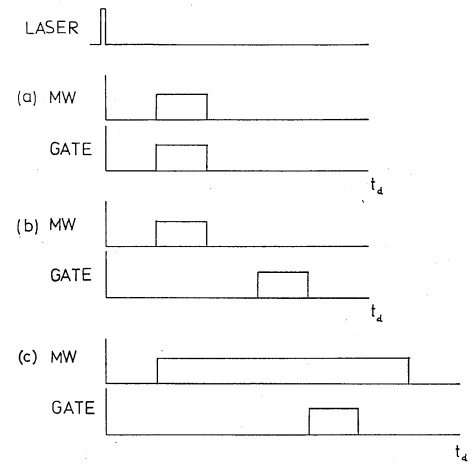

Fig. 10. Three types of timing of laser irradiation, microwave irradiation and gate for sampling against delay time, t_d.

recent TRODMR measurements.[32,34] Used TRODMR measurements are three types of timing of the laser pulse, the microwave pulse and the sampling gate, as shown in Fig. 10(a), (b) and (c). In these cases, the repetition frequency of the microwave pulse is half that of the laser pulse, so that microwave-induced changes in the luminescence are detected using a dual channel boxcar and digital lock-in detector. Street[34] used a continuous operation of the microwave which is similar to type (c). Depinna and Cavenett[32] introduced a method of TRODMR by frequency response spectroscopy to avoid accumulations due to long-lived states.[50]

Typical traces of TRODMR spectra observed in a-Si: H monitoring total emitted light are shown in Fig. 11, where a microwave pulse of 40 μs width is applied at 40 μs after a laser pulse (a nitrogen laser) is switched off, and the delay time of the sampling gate for observation of ODMR signals is changed from 40 μs to 140 μs after a laser pulse, following the detection sequence of type (b). The TRODMR spectra consist of a quenching signal in contrast with the steady state ODMR spectrum which is shown in Fig. 11 for comparison and consists of a narrow

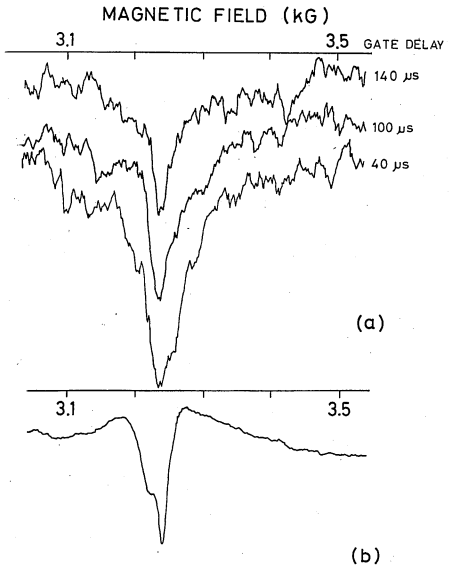

Fig. 11. (a) TRODMR spectra observed at 9.08 GHz and 2 K in a-Si: H No. 12 for various gate delay. (b) Steady state ODMR.[18]

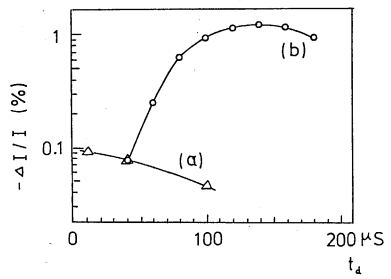

Fig. 12. ODMR intensity, $\Delta I/I$, at the peak position vs delay time. Curves (a) and (b) are the results obtained for timing of laser irradiation, microwave irradiation and gate (a) and (b) in Fig. 10, respectively.[18]

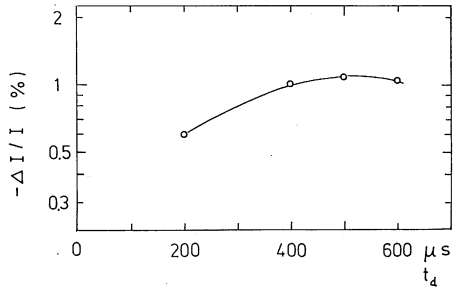

Fig. 13. ODMR intensity, $\Delta I/I$, at the peak position vs delay time obtained for timing of laser irradiation, microwave irradiation and gate (c) in Fig. 10.*

*K. Morigaki, P. Dawson and B. C. Cavenett: unpublished.

quenching line (the D_1 and D_2 lines) and a broad background line (enhancing). The peak intensities of the TRODMR are shown in Figs. 12 and 13 for three types of detection timing, (a), (b) and (c). In Fig. 12, curve (b) corresponds to the results of Fig. 11 and curve (a) was obtained by applying a microwave pulse of 40 μs width at various delay times after a laser pulse was switched off and by opening a sampling gate simultaneously with the microwave pulse. Figure 13 shows $-(\Delta I/I)_{ESR}$ as a function of delay time of sampling gate when a microwave pulse of 500 μs width was applied at 100 μs after a laser pulse was switched off.

The peak intensity of the quenching signal corresponds to $-(\Delta I/I)_{ESR}$ of dangling bond resonance. Curve (b) in Fig. 12 and curve in Fig. 13 are well understood by a model calculation described in the appendix (see the curves in Figs. 20 and 21). However, curve (a) in Fig. 12 is opposite in its time-variation to that calculated, i.e., the curve in Fig. 19. The reason for this discrepancy is not clear, but other agreements between model calculations and experiments seem to suggest that a previous model for spin-dependent nonradiative recombination at dangling bond centres described in §2.1 works well and that unthermalized electron-hole pairs (radiative electron centre-nonradiative hole centre (dangling bond centre) pair) contribute to quenching ODMR signals at 2 K. This conclusion is consistent with recent ODMR experiments by Depinna and Cavenett[32] and Street.[34]

As seen in Fig. 11, the ODMR signal becomes narrow with the increasing delay time of the sampling gate. This indicates that at the earliest time after a laser pulse is switched off, one deals with the closest electron-hole pairs (radiative electron centre-nonradiative hole centre

(dangling bond centre) pair), but with increased delay time of the sampling gate distant pairs contribute much more to the ODMR signal. Such behaviour of the ODMR signal with delay time has also been observed for donor-acceptor recombination in crystalline semiconductors.[51] Figure 11 shows that a broad quenching line is superposed on the narrow quenching line dealt with above. Although this background signal was thought to be the A line which appeared as a quenching line for TRODMR (see Appendix C), the precise origin of this background line is not clear at present. Depinna and Cavenett[32] have observed an enhancing ODMR signal at a delay time shorter than 50 μs, whereas Street[34] has observed it during $t_d = 10$ μs–1 ms (at 14 K), and a quenching ODMR spectrum at t_d shorter than 0.1 ms. The reason Morigaki *et al.*[18] did not observe an enhancing line may be that they used a GaAs tube for detection of emitted light (detection wavelength $\lesssim 900$ nm), while Depinna and Cavenett,[32] and Street[34] used a Ge detector (detection wavelength $\lesssim 1.9$ μm). Such enhancing ODMR line appears to be due to the A centre. Differences in TRODMR behaviour between the D_2 and A lines come mainly from a difference in T_1. According to Street,[34] the value of T_1 for D_2 and A centres at 10 K is $\gtrsim 20$ ms and ~ 50 μs, respectively; these values are used in the model calculation given in Appendix C. We should emphasize that this calculation was done for a given electron-hole pair, assuming the appropriate values of the parameters in rate equations. However, trapped electrons and holes (either at radiative or nonradiative centres) are distributed at random. Thus, we should take into account the distribution of trapped electron-hole pairs with respect to the separation of an electron and a hole, the extent of their wavefunction, and their energy levels in the bandgap region. Further theoretical and experimental study is required to understand the precise nature of dynamical aspects of the electron-hole pairs in a-Si: H.

§6. Nature of the Recombination Centres in a-Si:H

In discussing the nature of the recombination centres involved in the ODMR spectra, the D_2 centre with $g = 2.006$ is identified as being due to the dangling bond centres, as was mentioned in §4. According to the recent ODMR measurement by Street,[34] a high defect density sample containing the dangling bonds of 3.5×10^{17} cm^{-3} exhibits a quenching line with $g = 2.0055$, while a low density sample containing dangling bonds of 3×10^{15} cm^{-3} exhibits a quenching line very similar to the dangling bond resonance observed in the high defect density sample at low illumination levels. At high illumination levels, however, the observed quenching line consists of two components with $g = 2.0045$ and $g = 2.011$. Street identified a quenching line with $g = 2.0055$ as due to the dangling bond centres, and identified those lines with $g = 2.0045$ and $g = 2.011$ as due to conduction band tail electrons and valence band tail holes, respectively, because this ODMR spectrum resembles a light-induced ESR spectrum. He also interpreted these quenching lines as originating from the Auger process involving conduction band tail electrons and valence band tail holes. Our interpretation differs from Street's as follows: We consider that the D_1 and D_2 lines correspond to his quenching lines with $g = 2.011$ and $g = 2.0045$, respectively. The dangling bond resonance with $g = 2.0055$ presumably also contributes to the D_2 line. As mentioned, the D_1 and D_2 centres are nonradiative centres. It has previously been pointed out[8] that the light-induced electron centre with $g = 2.004$ which has been observed in light-induced ESR[52,53] and also in ODMR may be an electron trapped at a positively charged three-fold coordinated centre, T_3^+, whose wavefunction is formed from an sp^3 orbital, while the light-induced hole centre with $g = 2.013$ which has been observed in the light-induced ESR[52] and also in ODMR may be a hole trapped at a negatively charged three-fold coordinated centre, T_3^-, whose wavefunction is formed from a p orbital. This identification is based on a threefold coordination model[54,55] for structural defects, in which Si atoms are threefold coordinated by either sp^3-hybridized orbitals or p-orbitals. The electron trapped at T_3^+ and the hole trapped at T_3^- may each form a level above and below the midgap, respectively, and act as nonradiative centres.

The conduction band tail electrons contribute to radiative recombination but they do not seem to be observed in ODMR, as previously mentioned. Nature of the conduction band tail states is not clear. The potential fluctuation of the conduction band edge due to disorder associated with random Si network and random distribution of foreign atoms such as H and F may give rise to local minimum states[56] at which electrons are captured after band to band optical excitation.

The A centre that acts as the radiative centre has been identified as the trapped hole centre and its level has been estimated from the analysis of spectral dependences of the ODMR signals for various samples.[26,28] The detailed nature of this A centre is not known, but the recent optically detected electron nuclear double resonance[57] may provide information about it together with the nature of the D_2 centre.

As mentioned in §4, the dangling bond centres are created by prolonged light irradiation at low temperatures. Although the precise nature of such light-created defects is not clear, a possible model for such structural defects has been proposed.[58] Here, also, further study is required.

§7. Conclusion

In this paper, we have presented the principle of ODMR, i.e., how luminescence intensity changes at resonance for radiative recombination of distant electron-hole pairs and triplet excitons. Amorphous semiconductors have a disordered structure, so that the anisotropic properties of ODMR are generally obliterated, thus making it difficult to identify the recombination centres from the ODMR measurement. However, the time-resolved (TR) ODMR measurement is useful for such identification if ODMR signals are detected and the polarization of emitted light is monitored for a short time after the laser pulse is switched off. To do so, we should resolve the difficulty arising from the low sensitivity for detection of weak emitted light in a time scale of nanoseconds. The TRODMR technique has just begun to be used for amorphous semiconductors. Together with

TR luminescence measurements,[43,60] such ODMR measurements will elucidate the more detailed nature of trapping and recombination of electrons and holes generated by band to band excitation as well as the precise nature of the recombination centres.

Acknowledgements

I wish to thank Mr. Y. Sano and Dr. I. Hirabayashi with whom the steady state ODMR investigations have been carried out. The collaborations with Dr. B. C. Cavenett and Dr. P. Dawson on the TRODMR investigations in Hull have been very stimulating and to them I am very grateful. I am also grateful to Professor S. Nitta for a sample used in the TRODMR investigations and to Dr. B. C. Cavenett, Mr. S. Depinna and Dr. R. A. Street for sending me preprints of papers prior to publication. The model calculations in the appendix were done in collaboration with Dr. I. Hirabayashi, Mr. M. Nakayama and Ms. M. Yoshida to whom I am grateful.

Appendix A: Dependence of Luminescence Intensity on Excitation Intensity*

We consider the luminescence intensity as a function of excitation intensity on the basis of the rate equation model described in §2.1. From the steady-state solution for rate equations given by eq. (1), we obtain the luminescence intensity as a function of generation rate, G:

$$I\propto \frac{2GN\left[R^*+\frac{2}{T_1}\frac{x_e+x_h}{(1+x_e)(1+x_h)}\right]}{RR^*+(R+R^*)\left(\frac{1}{T_1}+2G\right)+\frac{1}{T_1}\left(\frac{1}{T_1}+4G\right)-\frac{(1+x_ex_h)\left(R+\frac{1}{T_1}\right)+(x_e+x_h)\left(R^*+\frac{1}{T_1}\right)}{T_1(1+x_e)(1+x_h)}}. \tag{A·1}$$

For the limiting cases of small and large G, this expression is approximated by the following equations. For a small G,

$$I\propto \frac{2GN\left[R^*+\frac{2(x_e+x_h)}{T_1(1+x_e)(1+x_h)}\right]}{RR^*+(R+R^*)\frac{1}{T_1}+\left(\frac{1}{T_1}\right)^2-\frac{(1+x_ex_h)\left(R+\frac{1}{T_1}\right)+(x_e+x_h)\left(R^*+\frac{1}{T_1}\right)}{T_1(1+x_e)(1+x_h)}}. \tag{A·2}$$

For a large G (optical saturation),

$$I\propto \frac{N\left[R^*+\frac{2(x_e+x_h)}{T_1(1+x_e)(1+x_h)}\right]}{R+R^*+\frac{2}{T_1}}. \tag{A·3}$$

In order to obtain relationship between generation rate and excitation intensity (laser power), we adopt a simple model which is appropriate to the present situation as follows:

The generation rate G defined in §2.1 is expressed by

$$G=\gamma_e n, \tag{A·4}$$

where γ_e is the trapping rate of free electrons by positively charged centres (electron traps) and n is the number of free electrons. We consider only a simple case where the rate equations are given by the following equations, neglecting spin statistics.

$$\begin{aligned}
\frac{dn}{dt}&=P-\gamma np-\gamma_e nN_e^+,\\
\frac{dn_e}{dt}&=\gamma_e nN_h^+-An_ep_h,\\
\frac{dp}{dt}&=P-\gamma np-\gamma_h pN_h^-,\\
\frac{dp_h}{dt}&=\gamma_h pN_h^--An_ep_h,
\end{aligned} \tag{A·5}$$

where P is the generation rate of free electron-hole pairs and is related to the excitation intensity, and γ, γ_h and A are the recombination rates of free electron-hole pairs, the trapping rate of free holes by negatively charged centres (hole traps) and the recombination rate of trapped electron-hole pairs, respectively, and p, n_e, p_h, N_e^+ and N_h^- are the numbers of free holes, trapped electrons and holes, positively and negatively charged centres, respectively.

For the limiting cases of small and large P, we have

$$G=\gamma_e n=P/N_e^+, \tag{A·6}$$

$$G=\gamma_e n=(\gamma_e/\gamma^{1/2})P^{1/2}, \tag{A·7}$$

respectively.

Thus the luminescence intensity, I, is given by eqs. (A·1) and (A·6) for weak excitation and by eqs. (A·1) and (A·7) for rather strong excitation (not for optical saturation). Figure 14 shows such a tendency of the I vs P curve.

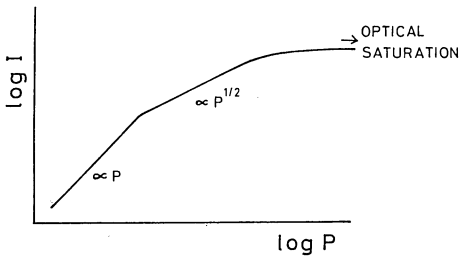

Fig. 14. Schematic diagram of log I (luminescence intensity) vs log P (generation rate of free electron-hole pairs).

Appendix B: Exact Solution of Rate Equations of Triplet Excitons

n_1 and n_3 are exactly calculated from the rate equations given by eq. (17) in the steady state condition as follows:

*K.Morigaki: Tech. Rep. ISSP, Ser. A, No. 1095, 1980 (unpublished).

$$n_1=\frac{G_1+A+B}{C+D+E}, \tag{B·1}$$

where

$$A=a\,e^{-\Delta E_1/kT}G_3\Big/\left(R_3+\frac{1}{T_1}+W_2-a\,e^{\Delta E_2/kT}\right), \tag{B·2}$$

$$B=\left[(W_1+a\,e^{-\Delta E_1/kT})+a\,e^{-\Delta E_1/kT}(W_2+a\,e^{\Delta E_2/kT})\Big/\left(R_3+\frac{1}{T_1}+W_2-a\,e^{\Delta E_2/kT}\right)\right]$$
$$\times G_2\Big/\left[\left(R_2+\frac{1}{T_1}+W_1+W_2-a\right)\left(1-\frac{(W_2+a)(W_2+a\,e^{\Delta E_2/kT})}{\left(R_2+\frac{1}{T_1}+W_1+W_2-a\right)\left(R_3+\frac{1}{T_1}+W_2-a\,e^{\Delta E_2/kT}\right)}\right)\right], \tag{B·3}$$

$$C=R_1+\frac{1}{T_1}+W_1-a\,e^{-\Delta E_1/kT}, \tag{B·4}$$

$$D=-a^2\,e^{-(\Delta E_1/kT-\Delta E_2/kT)}\Big/\left(R_3+\frac{1}{T_1}+W_2-a\,e^{\Delta E_2/kT}\right), \tag{B·5}$$

$$E=-\left[(W_1+a\,e^{-\Delta E_1/kT})+a\,e^{-\Delta E_1/kT}(W_2+a\,e^{\Delta E_2/kT})\Big/\left(R_3+\frac{1}{T_1}+W_2-a\,e^{\Delta E_2/kT}\right)\right]$$
$$\times\left\{\left[(W_1+a)\Big/\left(R_2+\frac{1}{T_1}+W_1+W_2-a\right)\right]+(W_2+a)a\,e^{\Delta E_2/kT}\right.$$
$$\left.\Big/\left[\left(R_2+\frac{1}{T_1}+W_1+W_2-a\right)\left(R_3+\frac{1}{T_1}+W_2-a\,e^{\Delta E_2/kT}\right)\right]\right\}$$
$$\Big/\left\{1-\left[(W_2+a)\Big/\left(R_2+\frac{1}{T_1}+W_1+W_2-a\right)\right]\left[(W_2+a\,e^{\Delta E_2/kT})\Big/\left(R_3+\frac{1}{T_1}+W_2-a\,e^{\Delta E_2/kT}\right)\right]\right\}, \tag{B·6}$$

$$a=1/T_1(1+e^{-\Delta E_1/kT}+e^{\Delta E_2/kT}), \tag{B·7}$$

n_3 is given by

$$n_3=\frac{Fn_1+H}{K}, \tag{B·8}$$

where n_1 is given by eq. (B·1) and

$$F=(W_1+a)(W_2+a\,e^{\Delta E_2/kT})+a\,e^{\Delta E_2/kT}\left(R_2+\frac{1}{T_1}+W_1+W_2-a\right), \tag{B·9}$$

$$H=G_3\left(R_2+\frac{1}{T_1}+W_1+W_2-a\right)+G_2(W_2+a\,e^{\Delta E_2/kT}), \tag{B·10}$$

$$K=\left(R_3+\frac{1}{T_1}+W_2-a\,e^{\Delta E_2/kT}\right)\left(R_2+\frac{1}{T_1}+W_1+W_2-a\right)-(W_2+a\,e^{\Delta E_2/kT})(W_2+a), \tag{B·11}$$

Appendix C: A Model Calculation of Time-Resolved ODMR

We present a model calculation of the relative change in luminescence intensity at resonance after the laser pulse is switched off. The rate equations for n_1, n_2, n_3 and n_4 (see §2.1 for definitions) used in the present calculation are the same as eq. (1) except for the generation rates which are given in the following. We take into account that free electron-hole pairs in the singlet states are generated by a laser pulse, i.e., a band to band excitation, and that free electron-hole pairs in the triplet states are also created from those in the singlet states through spin-flip processes. Bearing this in mind, we take the following expression for the generation rates of trapped electron-hole pairs in the singlet configuration states, G_s, and of those in the triplet configuration states, G_t.

$$G_s=\frac{1}{2}G, \quad \text{for } t\leqq t_{off}, \tag{C·1}$$

$$G_s=\frac{1}{4}G(1+e^{-(t-t_{off})/\tau_1})\,e^{-(t-t_{off})/\tau_2}, \quad \text{for } t\geqq t_{off}, \tag{C·2}$$

$$G_t=0, \quad \text{for } t\leqq t_{off}, \tag{C·3}$$

$$G_t=\frac{1}{4}G(1-e^{-(t-t_{off})/\tau_1})\,e^{-(t-t_{off})/\tau_2}, \quad \text{for } t\geqq t_{off}, \tag{C·4}$$

Generation rates are illustrated in Fig. 15. Since we are concerned with the slow decay component of the luminescence, we take a long decay of τ_2 for generation of trapped electron-hole pairs. The time of τ_1 is almost identical to the spin memory time, i.e., the spin-lattice relaxation time of generated electrons and holes. Thus the generation rate of the triplet configuration state, G_t, is assumed to have an expression given by eqs. (C·3) and (C·4). G_s and G_t decay at the same rate of $1/\tau_2$ after an appropriate time. This corresponds to the limiting case of the steady state condition, i.e., $G_s=G_t$, which is dealt with in §2.1.1.

First, we consider the case of the A centre resonance.

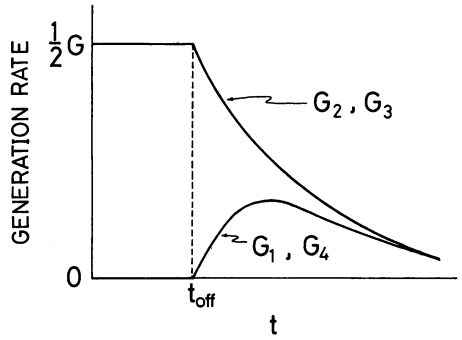

Fig. 15. Schematic diagram of generation rate, G_1–G_4, as a function of time.

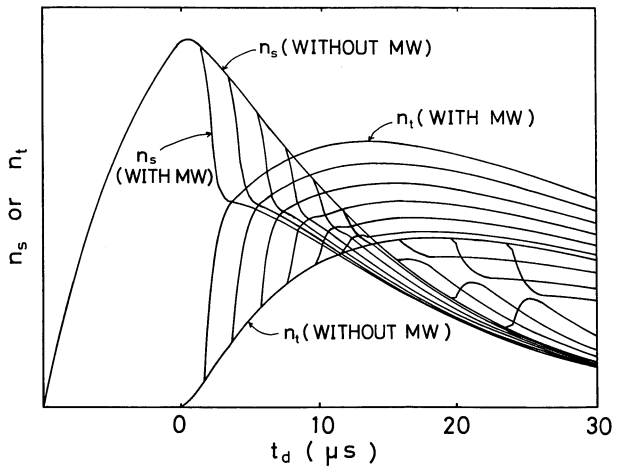

Fig. 16. n_s and n_t vs delay time, t_d with and without microwave irradiation for various delay times of microwave pulse. (see text). A microwave pulse of 2 μs width is applied at t_d=2, 4, 6, 8, 10, 12, 16, 20 and 24 μs.

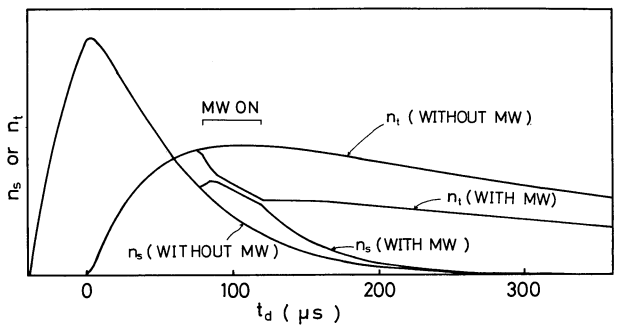

Fig. 17. n_s and n_t vs delay time, t_d, with and without microwave irradiation (see text).

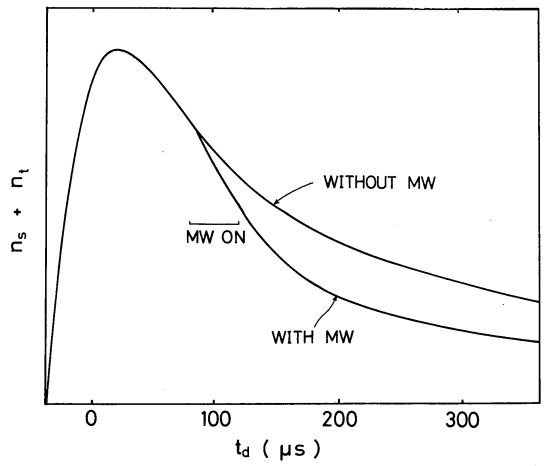

Fig. 18. n_s+n_t vs delay time, t_d, with and without microwave irradiation (see text).

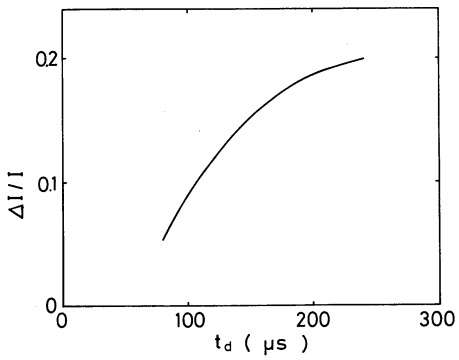

Fig. 19. $\Delta(n_s+n_t)/(n_s+n_t)$, i.e., $\Delta I/I$ associated with microwave irradiation plotted as a function of the delay time of the microwave pulse.

Since free electron-hole pairs in the singlet states are generated by a laser pulse, the population of the singlet configuration state, n_s, of the trapped electron-hole pair is greater than that of the triplet configuration state, n_t, just after the laser pulse is switched off. Thus, when ESR occurs between n_s and n_t, the population of n_s decreases and, as a result, the luminescence intensity also decreases. This corresponds to the case with the spin memory effect which is dealt with in §2.1.2. However, the situation is the opposite when n_t becomes greater than n_s. This is illustrated in Fig. 16, where n_s and n_t are calculated using the following parameter values: $G=1\times10^7$ sec^{-1}, $R=1\times10^5$ sec^{-1}, $R^*=1\times10^4$ sec^{-1}, $T_1=50$ μs (the value obtained by Street[34] at 10 K), $\tau_1=1$ μs, $\tau_2=10$ μs, $W_h=1\times10^6$ sec^{-1}, $W_e=0$, $t_{off}=10$ μs. The microwave pulse of 2 μs width is applied at t=2, 4, 6, 8, 10, 12, 16, 20 and 24 μs. Hereafter, t_d designates the time measured from just after the laser pulse is switched off, i.e., t_{off}. The curves of n_s and n_t cross each other at $t=14$ μs. Before and after this time, one obtains $(\Delta I)_{ESR}<0$ and $(\Delta I)_{ESR}>0$, respectively.

Secondly, we consider the dangling bond centre resonance. Following the model for nonradiative recombination[8] given in §2.1, the luminescence intensity is proportional to $(n_s+n_t)R_l$, where n_s and n_t designate the number of a radiative electron-nonradiative hole pair (see Fig. 2) with singlet and triplet configurations, respectively, participating in the nonradiative recombination and R_l is the radiative recombination rate. n_s and n_t are calculated using the following values of the parameters: $G=2.5\times10^6$ sec^{-1}, $R=2.5\times10^4$ sec^{-1}, $R^*=2.5\times10^3$ sec^{-1}, $T_1=40$ ms (Street[34] obtained the value of T_1 of $\gtrsim$20 ms at 10 K), $\tau_1=4$ μs, $\tau_2=40$ μs and $t_{off}=40$ μs. The microwave pulse of 40 μs width is applied after the laser pulse is switched off in the three ways shown in Fig. 10(a), (b) and (c). For example, Fig. 17 shows n_s and n_t calculated for the case with and without the microwave pulse which is applied during $t=80$ μs–120 μs. (n_s+n_t) for this case is shown in Fig. 18. $(\Delta I/I)_{ESR}$ which is proportional to the relative change in (n_s+n_t) associated with the microwave application, $\Delta(n_s+n_t)/(n_s+n_t)$, i.e., a relative change in the integrated intensity during the microwave pulse, is plotted as a function of the delay time of the

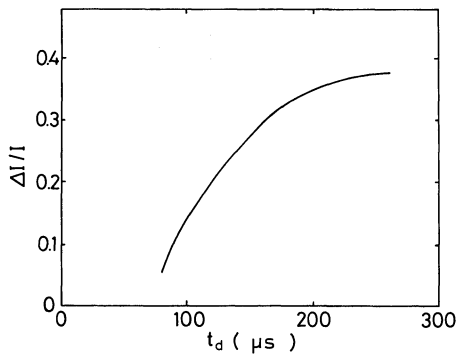

Fig. 20. $\Delta(n_s+n_t)/(n_s+n_t)$, i.e., $\Delta I/I$ associated with microwave irradiation at 80 μs–120 μs, plotted as a function of the delay time of the gate pulse (see text).

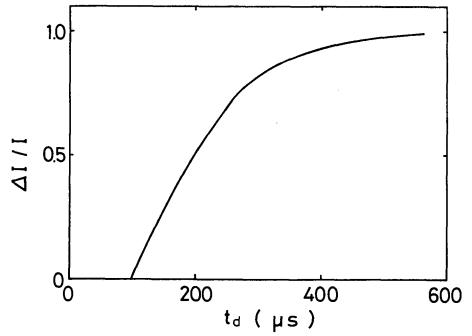

Fig. 21. $\Delta(n_s+n_t)/(n_s+n_t)$, i.e., $\Delta I/I$ associated with microwave irradiation at 100 μs–560 μs. t is measured from t_{off}.

microwave pulse after the laser pulse is switched off in Fig. 19.

Next, the microwave pulse is applied during $t=80$ μs–120 μs. Then, $\Delta(n_s+n_t)/(n_s+n_t)$, i.e., a relative change in the integrated intensity during the gate pulse of 40 μs width is plotted as a function of the delay time of the gate pulse after the laser pulse is switched off in Fig. 20.

Next, the microwave pulse is applied during $t_d=$ 100 μs–560 μs. $\Delta(n_s+n_t)/(n_s+n_t)$, i.e., $(\Delta I/I)_{ESR}$ is plotted as a function of t in Fig. 21.

The curves shown in Figs. 19–21 are compared with those measured for a-Si: H in the text. Details of this model calculation will be reported elsewhere.*

References

1) For a review, B. C. Cavenett: Adv. Phys. **30** (1981) 475.
2) J. R. James, J. E. Nicholls, B. C. Cavenett, J. J. Davies and D. J. Dunstan: Solid State Commun. **17** (1975) 969.
3) K. Murayama, K. Morigaki, S. Sakuragi and H. Kanzaki: J. Phys. Soc. Jpn. **41** (1976) 1617.
4) J. J. Davies, J. E. Nicholls and B. C. Cavenett: Semicond. & Insul. **4** (1978) 101.
5) D. Kaplan, I. Solomon and N. F. Mott: J. Phys. **19** (1978) L51.
6) D. J. Dunstan and J. J. Davies: J. Phys. C **12** (1979) 2927.
7) B. Movaghar, B. Ries and L. Schweitzer: Philos. Mag. **B41** (1980) 141.
8) K. Morigaki: J. Phys. Soc. Jpn. **50** (1981) 2279.
9) K. Murayama: Doctoral Thesis, Univ. of Tokyo, Tokyo, 1976.
10) K. Morigaki, P. Dawson and B. C. Cavenett: Solid State Commun. **28** (1978) 829.
11) B. C. Cavenett: *Proc. 15th Int. Conf. Physics of Semiconductors, Kyoto, 1980*, J. Phys. Soc. Jpn. **49** (1980) Suppl. A, p. 611.
12) S. P. Depinna and B. C. Cavenett: Phys. Rev. Lett. **48** (1982) 556.

*I. Hirabayashi, K. Morigaki and M. Yoshida: to be published.

13) S. P. Depinna and B. C. Cavenett: Philos. Mag. B, in press.
14) H. Suzuki: Doctoral Thesis, Univ. of Tokyo, Tokyo, 1982.
15) S. Depinna and B. C. Cavenett: Solid State Commun. **40** (1981) 813.
16) S. Depinna and B. C. Cavenett: Solid State Commun. **43** (1982) 25.
17) K. Morigaki, D. J. Dunstan, B. C. Cavenett, P. Dawson, J. E. Nicholls, S. Nitta and K. Shimakawa: Solid State Commun. **26** (1978) 981.
18) K. Morigaki, P. Dawson, B. C. Cavenett, D. J. Dunstan, S. Nitta and K. Shimakawa: *Proc. 14th Int. Conf. Physics of Semiconductors, Edinburgh, 1978* (Institute of Physics, London, 1978) p. 1163.
19) K. Morigaki, B. C. Cavenett, P. Dawson, S. Nitta and K. Shimakawa: Solid State Commun. **32** (1979) 795.
20) K. Morigaki, B. C. Cavenett, P. Dawson, S. Nitta and K. Shimakawa: J. Non-Cryst. Solids **35** & **36** (1980) 633.
21) D. K. Biegelsen, J. C. Knights, R. A. Street, C. Tsang and R. M. White: Philos. Mag. **B37** (1978) 477.
22) G. Lampel, M. Rosso and I. Solomon: Private communication. See also I. Solomon: *Amorphous Semiconductors*, ed. M. H. Brodsky (Springer-Verlag, Berlin, 1979) Chap. 7.
23) K. Morigaki, Y. Sano and I. Hirabayashi: Solid State Commun. **39** (1981) 947.
24) K. Morigaki, Y. Sano and I. Hirabayashi: J. Phys. Soc. Jpn. **51** (1982) 147.
25) Y. Sano, K. Morigaki, I. Hirabayashi and M. Konagai: Jpn. J. Appl. Phys. **21** (1982) L291.
26) K. Morigaki, Y. Sano, I. Hirabayashi, M. Konagai and M. Suzuki: Solid State Commun. **43** (1982) 751.
27) Y. Sano, K. Morigaki and I. Hirabayshi: Solid State Commun. **43** (1982) 439.
28) K. Morigaki, Y. Sano and I. Hirabayashi: Tech. Rep. ISSP, Ser. A, No. 1232 (1982); to be published in *Amorphous Semiconductor Technologies & Devices-1983* (Japan Annual Reviews in Electronics, Computers & Telecommunications, Ohmsha, Tokyo).
29) S. P. Depinna, B. C. Cavenett, I. G. Austin and T. M. Searle: J. Phys. **42** (1981) C4-323.
30) S. P. Depinna, B. C. Cavenett, I. G. Austin and T. M. Searle: Solid State Commun. **41** (1982) 263.
31) S. P. Depinna, B. C. Cavenett, I. G. Austin, T. M. Searle, M. J. Thompson, J. Allison and P. G. LeComber: Philos. Mag., in press.
32) S. P. Depinna and B. C. Cavenett: J. Phys. C **15** (1982) L489.
33) R. A. Street, D. K. Biegelsen and J. Zesch: Phys. Rev. B **25** (1982) 4334.
34) R. A. Street: Phys. Rev. **B26** (1982) 3588.
35) M. Kastner, D. Adler and H. Fritzsche: Phys. Rev. Lett. **37** (1976) 1504.
36) K. Murayama, H. Suzuki and T. Ninomiya: J. Non-Cryst. Solids **35** & **36** (1980) 915.
37) S. P. Depinna, B. C. Cavenett, T. G. Austin and T. M. Searle: J. Non-Cryst. Solids **35** & **36** (1980) 933.
38) S. G. Bishop, U. Strom and P. C. Taylor: Phys. Rev. B **15** (1977) 2278.
39) F. Mollot, J. Cernogora and C. Benoit à la Guillaume: J. Non-Cryst. Solids **35** & **36** (1980) 939.
40) D. K. Biegelsen and R. A. Street: Phys. Rev. Lett. **44** (1980) 803.
41) H. Suzuki, K. Murayama and T. Ninomiya: J. Phys. Soc. Jpn. **46** (1979) 693.
42) R. A. Street and N. F. Mott: Phys. Rev. Lett. **35** (1975) 1293.
43) For a review, R. A. Street: Adv. Phys. **30** (1981) 593.
44) M. H. Brodsky and R. S. Title: Phys. Rev. Lett. **23** (1969) 581.
45) K. Morigaki, I. Hirabayashi, M. Nakayama, S. Nitta and K. Shimakawa: Solid State Commun. **33** (1980) 851.
46) J. I. Pankove and J. E. Berkeyheiser: Appl. Phys. Lett. **37** (1980) 705.
47) I. Hirabayashi, K. Morigaki and M. Yoshida: Sol. Energy Mater. **8** (1982) 153. Further references therein.
48) P. Dawson and B. C. Cavenett: J. Lumin. **18/19** (1979) 853.

49) P. Dawson, B. C. Cavenett and G. Sowersby: Solid State Electron. **21** (1978) 1451.
50) D. J. Dunstan, S. P. Depinna and B. C. Cavenett: J. Phys. C **30** (1982) L425.
51) D. Block and R. T. Cox: J. Lumin. **24/25** (1981) 167.
52) J. C. Knights, D. K. Biegelsen and I. Solomon: Solid State Commun. **22** (1977) 133.
53) R. A. Street and D. K. Biegelsen: Solid State Commun. **33** (1980) 1159.
54) D. Adler: Phys. Rev. Lett. **41** (1978) 1755.
55) S. R. Elliott: Philos. Mag. **B38** (1978) 325.
56) D. J. Dunstan and F. Boulitrop: J. Phys. **42** (1981) C4-331.
57) Y. Sano, K. Morigaki and I. Hirabayashi: *Proc. 16th Int. Conf. Physics of Semiconductors, Montpellier, 1982*, Physica B, in press.
58) I. Hirabayashi, K. Morigaki and S. Nitta: Jpn. J. Appl. Phys. **19** (1980) L357.
59) K. Arai and H. Namikawa: Solid State Commun. **13** (1973) 1167.
60) I. Hirabayashi, K. Morigaki and S. Nitta: J. Phys. Soc. Jpn. **50** (1981) 2961.